Enhanced visible light photoactivity and charge separation in TiO2/TiN bilayer thin films

Houssam Fakhouri, Farzaneh Arefi-Khonsari, A.K. Jaiswal, Jérôme Pulpytel

Enhanced visible light photoactivity and charge separation in TiO_2/TiN bilayer thin films

H Fakhouri[1,2*], F Arefi-Khonsari[1,2*], A K Jaiswal[1,2], and J Pulpytel[1,2]

[1] Sorbonne Universités, UPMC Univ Paris 06, UMR 8235, Laboratoire Interfaces et Systèmes Electrochimiques, F-75005 Paris, France.

[2] CNRS, UMR8235, LISE, F-75005 Paris, France

**** Corresponding author.***
E-mail addresses: farzi.arefi@upmc.fr (F Arefi-Khonsari), houss.fakhouri@gmail.com (H Fakhouri)
Phone: +33 147276823

Abstract

Multi-layered thin films of TiO_2 and TiN were created by RF reactive magnetron sputtering and were compared with homogeneous thin films of N doped TiO_2 having the same thickness. The crystalline, chemical, optical and photoactive properties were measured and discussed in detail. The number of bilayers was kept constant either 9 or 18 bilayers, but the overall composition (TiN to TiO_2 ratio) was varied. The TiN and TiO_2 layer thicknesses were controlled systematically in order to produce films with TiN to TiO_2 ratio ranging from 5% to 28%. The TiN/TiO_2 ratio was controlled for both bilayers in order to get the best synergic effect of light absorption/reflection and charge separation based on the generation of the photo-electrochemical current and the photocatalytic activity under UV and visible light. A maximum photocurrent generation was found for thin films having a TiN/TiO_2 ratio of 21% and 28% for the 9 bilayer and the 18 bilayer films, respectively. The superiority of the configuration of the 18 bilayer has been confirmed by studying the photocatalytic activity. The photoactive improvement of the bilayered thin films as compared to non-doped TiO_2 is the result of the enhanced charge separation at the heterogeneous junction, interfacial effects between TiN and TiO_2, which is found to depend on the thickness of the TiN layers. Electronic as well as optical approaches have been presented to explain the superiority of the bilayers strategy. This study has shown that a bilayered morphology of TiN and TiO_2 can significantly enhance the photocatalytic and photoelectrochemical behavior of TiO_2 under visible light illumination conditions which is applicable to numerous fields.

Keywords: TiO_2, titanium nitride, bilayer, charge separation, anatase, magnetron sputtering, heterogeneous junction, photocurrent, photocatalysis.

1. Introduction

TiO_2 has been used as an effective UV light photocatalyst for many decades. In recent years, the applications for TiO_2 have grown to include sensors, water splitting for hydrogen generation, dye sensitized solar cells, and self-cleaning surfaces. However, for many photoactive applications, TiO_2 by itself has several deficiencies that will not allow it to be a commercially viable option for large-scale integration. The band gap energy for anatase TiO_2 is E_g = 3.2 eV, which corresponds to an absorption wavelength of λ = 388 nm. This makes TiO_2 a suitable candidate for UV-based photoactive systems, but not a practical long-term solution to use the solar spectrum of the sun to initiate visible light induced photo-reactions. In addition, the relatively short lifetime of the photogenerated electron-hole pairs in TiO_2 obstructs the advancement of its applications due to very fast recombination, which is in the order of some μs [1]. The electrons and holes are used in separate reduction and oxidation reactions at the TiO_2 surface, so extending the lifetime of each charge carrier is vitally important to improving the efficiency of TiO_2 as a functional photoactive material. Therefore, several methods have been developed to improve the overall efficiency of TiO_2 by adjusting the structural, morphological properties and the composition of the material. Much of the recent research focusing on the improvement of the functionality of TiO_2 has centered on increasing the absorption range to include visible light, as well as increasing the lifetime of UV generated electron-hole pairs [2-4]. One of the most popular methods to increase the visible light absorption in TiO_2 is to dope the material with non-metals such as sulfur [5], carbon [6], and nitrogen [7-10]. However, reducing the band gap of TiO_2 by doping could affect the crystal phase, composition and the electronic structure of TiO_2 which is critical for the optoelectronic performances. Doping TiO_2 with nitrogen has received considerable attention due to the small ionic radius of nitrogen, and the desired energy band levels which can be introduced substitutionally, interstitially, or both within the band gap of TiO_2 [11]. Asahi et al. [8] explored N-doped TiO_2, and through theoretical (DOS calculations) and experimental results (by using different analytical techniques of characterization of the doped films such as XPS, UV-Vis, and photocatalytic activity), they were able to determine that nitrogen is the best suited element to improve TiO_2 photo-functionality in the visible light region. Since then, many studies have shown the viability and success of N-doped TiO_2 as a visible light photoactive material.

Other ways to improve the photoactive properties of TiO_2 include coupling it with other semi-conductors or metals [12-15]. When TiO_2 is in contact with other semi-conductors that have higher conduction band position as compared to TiO_2, an electronic heterostructure is formed at the interface, which can trap electrons in the conduction and localize holes in

valence bands, extending the lifetime of the photogenerated charge carriers. This can allow the photogenerated electrons in the TiO_2 conduction band to travel to the secondary semi-conductor, or allow photogenerated holes to transfer to the TiO_2 valence band. Similarly, when TiO_2 is in contact with a material having higher Fermi level, a Schottky barrier is formed which is proportional to the difference between the Fermi energy level of TiO_2 and the hosted material. This barrier is an electric field that can affect charge carriers in a nearby region and creates the space charge layer which corresponds to the band bending region. This can further increase the effective lifetime of the photogenerated electron-hole pair and has shown the ability to significantly increase the photocatalytic and photoelectrochemical properties of these structures [16].

In this study, we optimized a unique organization of TiO_2/TiN bilayer thin films that show significant enhancement in visible light photocurrent generation and photocatalytic activity compared to similar films made in a previous work [17]. Films were deposited with 9 bilayers, and 18 bilayers having all the same total height (500 ± 50 nm) and with different thicknesses of the TiN and TiO_2 layers. By designing each film with the particular amount of bilayers, we were able to create 17 and 35 TiN/TiO_2 heterojunctions in each respective sample, and allowing the ratio of TiN to TiO_2 to vary between 5% and 28% throughout each film. The films were then annealed at $T = 450^oC$ for 2 hours and their crystalline structure was measured in order to examine the interactions between the two phases of TiN and TiO_2 constituting the film. The photocatalytic and photoelectrochemical properties were measured for these films, which displayed a distinct response in photocurrent generation under UV and visible light irradiation, dependent on the thickness/number of layers. These results demonstrate a unique and simple way to improve the photoactive properties of TiO_2 for many applications.

2. Experimental

TiO_2 and TiN films were deposited in the same RF magnetron sputtering chamber. The depositions for the bilayer films were carried out successively under the same vacuum and without opening the chamber between depositions of the sub layers. The base pressure for depositions was $p \sim 3$ to 7 x 10^{-6} torr, while the total working pressure was kept constant at 3.5 mtorr. All films were deposited using a metallic Ti target sputtered in a reactive gas atmosphere, containing Ar + O_2 for TiO_2 films and Ar + N_2 for TiN films. The argon gas flow rate was fixed at 35 sccm for both depositions, while the O_2 and N_2 flow rates were fixed at 2 and 1.2 sccm for TiO_2 and TiN depositions, respectively. The RF power of the cathode was 200 W (DC bias voltage of about -148 V) for all the depositions in order to

minimize the target poisoning effect. The substrate holder was maintained at 300°C and no bias was applied. The distance between the substrate holder and the target was fixed at 100 mm.

Prior to each multi stack deposition the target was pre-sputtered in argon atmosphere for 10 minutes to remove any contamination from the target surface. The films were deposited on several substrates including electro-polished stainless steel, Si (100) wafers and ordinary microscope glass slides. Prior to deposition, the substrates were ultrasonically cleaned with acetone, ethyl alcohol and then de-ionized water for 20 minutes each.

Table 1 presents the deposition parameters for the 9 and the 18 bilayer, including the nominal estimated thickness of each TiO_2 and TiN layers. The structure of the stacked films is completed with the deposition of a TiO_2 layer of 30 nm to 40 nm.

The crystal structure of deposited thin films was characterized by X-ray diffraction XRD (X'Pert Pro PW3040-Pro, Panalytical Inc.) using a Cu Kα1 (λ = 1.5418 Å) X-ray radiation source in Bragg-Brentano (θ-2θ) configuration. X'Pert High Score pattern processing was used to collect and process the data. XPS analyses were performed using a Thetaprobe spectroscope (by Thermo Scientific). The source employed was Al Kα monochromated radiation at a power of 140 W.

Photo-electrochemical measurements PEC were performed at room temperature in a three-electrode cell, using Solartron SI 1287 as electrochemical interface. The reference and counter electrodes used during the PEC measurements were an Ag/AgCl electrode (CHI Instruments/saturated KCl) and a mesh Pt electrode, respectively. Electrochemical cell was filled with an electrolyte of Na_2SO_4, 1 M (Merk). 125 W white lamp as well as 500 W halogen lamp (both from PHILIPS) have been used to irradiate the samples with UV and Visible lights, respectively, for the photocurrent measurement. A UV filter has been used to cut off all the UV irradiation for the visible light measurements. Photocatalytic and photo-induced hydrophilic properties were studied by pre-contaminating the surface of the coatings, with oleic acid (97%, Acros Organics) for 24 hours, then by following the variation of the wettability of the coatings under white light irradiation. The wettability was estimated by measuring the contact angle of a droplet of 6µm size deionized water on the surface of the TiO_2/TiN bilayers. The study of the photocatalytic activity was completed by following the discoloration of an aqueous solution of Rhodamine B (Acros Organics), having an initial concentration of 5 ppm, in presence of the thin films and under different irradiation conditions. The treated volume of the dye was 5 ml, the dye and the thin coatings (photocatalytic material deposited on glass substrate having initial size of 9x26 mm) were put

in a sealed UV grade cuvette with the photocatalytic material opposite to the light. Then the degradation of Rhodamine B was followed by measuring the variation of the photo absorbance, of the dye, with the time.

3. Effect of the interface between the TiN and TiO_2 (electronic approach)

It is well known that titanium nitride is a hard and conductive material, especially when it is deposited at lower pressure and substrate temperatures higher than 200°C [18]. The work function of TiN is found to be about 3.5 to 4.4 eV [19] depending on the preparation method, the stoichiometry and the crystallinity. TiO_2 can have a work function of 4.50 eV to 4.66 eV and an electron affinity of 4.2 eV [20-22], permitting TiN to have higher Fermi level and higher charge density as compared to TiO_2, as presented in Fig. 1 (a). This allows us to assume that, when stacking TiN in perfect contact with TiO_2, the Fermi level of TiO_2 should shift to be at the same energy level as that of TiN leading to the formation of ***Schottky barrier*** and band bending near the TiO_2/TiN interface as shown in Fig. 1 (b). However, the presence of the Ohmic contact could not be excluded. The band bending region within the TiO_2 layer is called the ***space charge*** and its width is proportional to the difference between the Fermi energy level of TiO_2 and the TiN (typically, it is reported to have a width of 2nm to 70nm) [23-24]. Depending on the quality of the ohmic contact and the charge space region, a charge transfer can take place at the interface between TiO_2 and TiN to assure the electronic equilibrium, resulting in a configuration with the curvature of the electronic bands. In this TiO_2 space charge layer, a static electric field can affect the charge carriers in a nearby region, reducing the probability of electron-hole recombination, which can further increase the effective lifetime of the photo-generated electron-hole pairs.

4. Results and discussion

4.1. Crystal Structure of TiO_2/TiN Bilayer Thin Films

The crystallographic diffractograms of the 9 and 18 bilayer samples are presented in Fig. 2 (a) and (b), respectively. In order to effectively demonstrate the differences in the crystallinity as a function of the deposition parameters, the XRD pattern of TiO_2 is presented as well in Fig. 2 (a). TiO_2 is well crystallized in the anatase phase having the preferential orientation of (101) at $2\theta = 25.4°$ and (004) at $2\theta = 37.8°$. As the TiN layer is introduced, the overall shape of the XRD pattern changed, the anatase peak of the (004) orientation decreased very fast, even with lower nominal ratio of TiN, indicating a decrease in the crystallinity and/or a sharp shrinking of the anatase crystal in the preferential (004) orientation for these particular films. The peak at $2\theta = 25.4°$ (101) became gradually wider and having lower

intensity as the ratio of TiN increased from 5% to 28% in the multi stack. This is a clear indication of either (i) the decrease in the crystal size of the anatase phase when the ratio of TiN increases (see next section) and/or (ii) a slight deformation in the TiO_2 crystal due to the presence of TiN, in fact, many works reported a crystal modification when substituting nitrogen into the anatase TiO_2 crystal or the presence of oxy-nitride phases [25-26]. In the case of 9 bilayers, a diffraction peak appeared at 36.0° at higher TiN ratio (TiN>21%), this diffraction peak is representative of the cubic (111) orientation of TiN crystal and its intensity is proportional to the ratio of TiN in the bilayer coating. The latter samples had much wider diffraction peaks for the anatase phase that means there was a dramatic deformation in the anatase crystal of TiO_2. However, we didn't observe any diffraction peak of TiN in the 18 bilayer samples which means that the thickness of the TiN layer was still lower than the detection limit of the diffractometer. The latter hypothesis is in agreement with the nominal values of the thickness of the TiN layers as reported in Table 1. The thickness of TiN increases with the increase of TiN ratio, but it is the opposite for that of TiO_2.

To summarise, the TiO_2 in the bilayer configuration is more crystallized in the preferential orientation of the anatase (101) rather than the anatase (004), the crystals of TiN became clear only in the 9 bilayers having the higher ratio of TiN.

4.2. Effect of TiN layer on the crystal size of TiO_2

The crystal size of TiO_2, in the different bilayer coatings, has been determined using the Scherrer formula with the parameters of the diffraction peak of the anatase (101). Fig. 3 describes the changes of the crystal size of the anatase phase (101) at 25. 4°, for both the 9 and the 18 bilayers, as a function of the ratio of TiN. This plot confirms the decrease of the crystal size of the anatase phase with the ratio of TiN, which is more pronounced in the case of the 9 bilayers. This difference between the two types of bilayers could be, again, explained by the higher thickness of the TiN layers in the 9 bilayers as compared to the 18 bilayers, for the same ratio of TiN. In fact, as the TiN is a hard material at the interface of the TiO_2 layer, it can limit the growing and crystallization of the anatase phase especially when post annealed, which leads to the formation of smaller anatase crystals at higher TiN ratio. The decrease in the crystal size of the anatase phase can also be related to the effective decrease in the thickness of the TiO_2 layer when the TiN ratio% increases. The TiN layer can also induce a strain on the anatase crystal, which can be justified by the relatively broadened diffraction peaks of the anatase (101) at higher TiN ratios.

4.3. XPS surface analysis

XPS surface analysis was used to determine the composition of each film at the surface of each bilayer stack. Theoretically, as the upper layer of each multi stack film is composed of a 30~40 nm thick film of pure TiO_2, the XPS data should provide only the characteristics of this thin layer, but it can also show the influence of the deeper layers on the superficial TiO_2 one (such as the nitrogen diffusion to the surface, the change in the electronic structure on the surface,... etc). In order to investigate the effect of the number of bilayers, we added a supplementary section in which we extended the study of XPS analysis to include 9, 18, 27, 36 and 45 bilayers, having the same ratio of TiN, as compared to pure TiO_2 thin film.

4.3.1 Ti 2p and O1s peaks observation and analysis

Fig.4 presents the different trends of the Ti 2p spectra as well as the O 1s and N 1s core level spectras, for samples prepared at a fixed TiN ratio (21%) within the stack, as we change the number of layers.

Besides than the Ti $2p_{1/2}$ peaks, the spectra of pure TiO_2 and stacked TiO_2/TiN films exhibited a Ti $2p_{3/2}$ peak at binding energies between 458.5 and 459 eV, which is in agreement with the values reported for anatase TiO_2 [27-31]. This indicated that the titanium was in a fully oxidized state of Ti^{4+} in the stacked films (O–Ti–O bonds of anatase) [32-33]. This conclusion is confirmed by considering the distance between the peaks of Ti $2p_{3/2}$ and O1s which was about 71.4 eV, this distance did not change when changing the number of layers or the ratio of TiN in the multistakes.

On the other hand, as the number of layers increased, the Ti 2p peak shifted towards lower binding energies, this shift was even higher when the number of layers increased (459 eV to 458.5 eV, see the supplementary section), which means that there is a change in the chemical environment for the titanium when the number of layers increased. This shift could be explained by many reasons: (i) partial reduction of the titanium cations associated with the formation of oxygen vacancies in the lattice, (ii) the bonding of Ti to lower electronegative species as compared to oxygen, such as the formation of Ti—N bonds within the TiO_2, or (iii) the change of the electronic affinity of the stacked TiO_2/TiN material.

The electrostatic charging has been already corrected by setting the C 1s spectrum at 285 eV and applying the resulted shift to all the other spectra. However, the partial reduction of Ti could be excluded as the same shift has been detected in the O 1s peaks. Indeed, the

energy shift between Ti $2p_{3/2}$ and O 1s was about ***71.4 eV***, which was the same for all the bilayer films, this means that the stoichiometry of the topmost TiO_2 layer was the same for all of the analysed samples. Also, the presence of substitutional N species (Ti—N bonds) could be also excluded since the N 1s spectra (Fig.4 (c)) presents a broad nitrogen peak centred around 400 eV corresponding to trapped chemisorbed nitrogen molecules [11][31][34-36]. Indeed titanium nitride (Ti—N) and substitutional N species such as (O—Ti—N) bondings are usually detected at binding energies lower than 398eV [26][28][31][33][36-40]. The incorporation of substitutional nitrogen species could be favoured only in partially reduced titanium oxide networks, so the Ti—N species could appear only when the oxide is defective at the surface of the upper TiO_2 layer.

Therefore, the change in the electronic affinity is the main reason for the shift in Ti 2p peak as the number of layers changes. The electronic affinity of pure TiO_2 is supposed to be slightly higher than 4.2 eV as the conduction band of TiO_2 is at 4.2 eV (as compared to the vaccum level) [20] as seen on Fig. 1. When the number of bilayers increases, the thickness of each TiN layer in the stack decreases and the space charge capacity, within TiO_2, should change. The variation in the space charge affects the total electronic affinity of the stacked TiO_2/TiN film. Laidani et al. [41] already proposed that the shift in binding energy could result from the variation of the position of Fermi level with respect to the core lines in the case of TiO_2 having intrinsic defects.

It is useful to mention that the photo-emitted electrons that have escaped into the vacuum of the XPS instrument are those which originate from less than 5 to 10 nm from the top of the material (TiO_2 layer). All of the deeper photo-emitted electrons, which were generated as the X-rays penetrated 1– 5 micrometers in depth of the material, are either recaptured or trapped in various excited states within the material.

The same samples also exhibited a main O 1s peak at 529.8 eV to 530.3 eV (assigned to O—Ti—O bonds) which are reported to be the typical oxide peak in titania [30-31].

4.3.2. O1s and N1s peaks deconvolution and analysis

Fig.5 presents an example of XPS spectrum of O 1s core for the 18 bilayers sample (having TiN ratio of 21%) after deconvolution. The presence of the O 1s shoulder at higher binding energies, between 531 eV and 533 eV, suggests: (i) the presence of hydroxyl (–OH) groups on the surface of these samples (contribution of Ti—OH bonds) [43], and/or (ii) the presence of C—O bonds (533 eV) and C=O bonds (531.5 eV) as a surface contamination [41-

42], and /or (iii) the formation of Ti—O—N bonds on the surface of TiO_2 due to interstitial incorporation of nitrogen [31].

The last suggestion concerning the attribution of the chemical shift of O1s can be excluded as no peaks, in the N 1s core level spectrum, corresponding to interstitial N (at 402 eV) or even substitutional N (at 396~398 eV) were detected on the surface of the bilayer coatings (see Fig. 4 (c)) [11][40]. The presence of hydroxyl groups and also the hydrocarbon contamination are both possible especially as the N 1s spectra (Fig.4 (c)) present a large nitrogen peak centred at about 400 eV, corresponding to trapped chemisorbed nitrogen molecules N_2 and/or some O—N species, due to nitrogen contamination from the residual nitrogen gas in the sputtering reactor or from the ambient atmosphere.

Finally, we can summarize these analytical results by two main conclusions, first, the limited diffusion of nitrogen between the TiN and TiO_2 layers, nitrogen was only detected in chemisorbed sites at the surface of the upper TiO_2 layer with no direct bonding between Ti an N. Secondly, the possible change in the electronic affinity of the final stacked material when increasing the number of layers (TiO_2 and TiN).

4.4. Photo-electrochemical properties

To investigate the photoelectrochemical activity under different irradiation conditions (dark, UV light and visible light) the photocurrent response has been measured at a fixed DC bias 0.5 V in intermittent intervals (30 sec white-light irradiation and 30 sec dark, $t_{on} = t_{off} = 30$ sec) for 210 seconds. From that point (after 210 sec), a UV filter was used to cut the UV irradiations of the white light, in order to measure the photocurrent generated under visible irradiation from the same lamp. These measurements have been done for all the samples using Ag/AgCl as a reference electrode. As discussed by A. Fujishima and K. Honda [44], the photo-induced oxidation reactions at TiO_2 surfaces are mainly due to water splitting and the value of photocurrent can therefore be directly related to the kinetics of O_2 generation.

Fig.6 (a) and (c) present the photocurrent generation under white-light irradiation for the 18 and 9 bilayer films, respectively, prepared at different TiN thickness ratios (5% to 28% as compared to TiO_2 layers in the stacked films). Dark photocurrent (no light irradiation) was less than 1 µA for all these samples. Fig.6 (b) and (d) present the evolution of the measured photocurrent when we inserted the UV filter after 210 seconds, so only visible light reached

the film surface. These figures can give us a clear idea about the evolution of the electrochemical photo-activity under the different illumination conditions.

The 9 and 18 bilayer films gave the most similar photocurrent density to pure TiO_2 thin films under UV light, but the bilayers give more efficiency under visible irradiations (less than 1 µA for TiO_2 and 4~23 µA for the 18 bilayer depending on the TiN ratio).

Fig.7 shows the measured values of the photocurrent at 0.5 V, after the stabilization period (30 sec), measured under white light (black) and visible light (red) irradiations for both type of bilayers (9 and 18 bilayers) versus the TiN ratio in the films. In this study, the 18 bilayers multistack is still more efficient to generate higher photocurrent than the 9 bilayers under white light (UV) as well as visible light irradiation, which is consistent with our previous results [17]. The 18 bilayers could generate a photocurrent up to 2.5 times higher than that generated by the 9 bilayers. In the case of the 18 bilayers, the photo-induced current increased steadily (up to 400 µA in the white light and 23 µA in the visible light) as the TiN ratio increased up to 28%. But with the 9 bilayers, the photo-generated current showed a maximum (154 µA in white light and 13.5 µA in visible light) for a TiN ratio of 21%. A further increase in the TiN ratio leads to a decrease in this photo-activity.

Many reasons could be responsible for this dramatic decrease in the photo-activity of the 9 bilayers when the % TiN reached 28%. We believe that the TiN layer thickness is a decisive parameter which determined the efficiency of the bilayer coatings, deposited at the particular pressure of 3.5 mtorr which gives rise to dense films [11]. Indeed, when the number of the layers increases at fixed TiN ratio (18 as compared to 9), the thickness of the TiN layer decreased as well as the thickness of TiO_2 layer (Table 1). The photoactive material (in the bilayer film) is the TiO_2 layers, the increase in the thickness of the TiN layer is accompanied with a decrease of the TiO_2 layer one for the same number of layers. On the other hand, we can assume that thicker TiN layers (conductive material) could induce electron-hole recombination leading to a reduction in the photoactivity.

From Table 1, the maximum TiN thickness in the 18 bilayers (TiN ratio of 28%) is 8 nm which is still much thinner than the 11 nm of TiN thickness in the 9 bilayers (TiN ratio of 21%) after which the photocurrent decreases. The results here show that the best photocurrents have been obtained for a thickness of TiN layer which was less than a critical value, between 11 nm and 15 nm. It seems that when the TiN thickness exceeds this critical value, there should be a dramatic decrease in the photo efficiency, however since the TiO_2

thickness decreases when the TiN thickness increases, it is difficult to conclude. In fact, the TiN layer could have the following effects: first, the ratio of TiN (in the bilayer film) affects the charge space region. Secondly, the increase of the TiN ratio (apparently above a certain value) decreases the UV and visible light absorption within the TiO_2 layer due to optical losses associated with the internal reflections at the TiO_2/TiN film interfaces (see the supplementary section).

4.5. Memory effect and transient time constant in the electrochemical photo response

The most interesting phenomena observed in the bilayer films was the evident photocurrent relaxation observed when switching from white-light to visible irradiation (at 210 sec) as shown in Fig. 6 (b) and (d). The stabilization of the visible light photocurrent (and dark) takes place after extending the time from cutting off the UV irradiations. This is a direct reflection of the charge separation efficiency of the bilayer array where the recombination rate of the charge carriers could be reduced, as compared to pure or some doped TiO_2 films, due to electron transfer from TiO_2 to the TiN layer. With the 9 bilayers, the visible light photocurrent is stabilized after 50 seconds from the instant when the UV filter is inserted (for samples having 21% TiN ratio). This relaxation time is even higher in the case of the 18 bilayer with the samples having up to 28% TiN ratio (more than 90 seconds). Here again, the charge recombination rate was found to be efficiently reduced with the 18 bilayers as the TiN ratio increased, the visible photocurrent (*after a white light illumination*) was increased from 1µA up to 23 µA when the TiN ratio increased from 5% to 28% (see Fig.7 (b)).

The relaxation of the measured photocurrent could be modulated in the following equation:

$$\zeta = \frac{I(t) - I_{st}}{I_0 - I_{st}} = e^{\left(-t/\tau\right)} \quad (1)$$

Where τ is a transient time constant which depends on the recombination rate between the photogenerated electron-holes, ***I(t)*** is the measured current at time ***t,*** I_{st} is the stationary current after stabilization, I_0 is the initial current at the beginning of the transient period when we stopped the irradiation (or switched from white to visible light). Based on equation 1, the values of $\ln(\zeta)$ were plotted vs time (an example is presented in the supplementary information) and we used a linear fitting to extrapolate the points and find the slope of the resulted plot which is the inverse of τ. Table 2 illustrates the calculated values of the transient time τ for the 9 and 18 bilayers at different TiN ratios.

The results show that when the thickness of TiN in the bilayer is below the critical values (*11 to 15 nm*), the transient time is increased when the TiN ratio increases. This means that the recombination time is reduced when the TiN thickness increases but remains below the critical thickness. The 18 bilayers multistack having 28% of TiN/TiO_2 thickness seems to reduce the recombination between the photo-generated carriers more than 10 times as compared to the 18 bilayers having TiN ratio of 5%.

4.6. Photocatalytic activity

Fig. 8 presents the variation of the wettability under white light irradiation, using deionized water, of the different thin coatings after contamination with oleic acid. It is important to mention that all the freshly deposited thin films were hydrophilic having water contact angle of less than 10°. After contamination, the water contact angle increased for all the samples in the same way to reach about 72°±4°. Under irradiating with white light, the photo-induced hydrophillicity was considerably higher for the higher ratio of TiN of both 9 and 18 bilayers. The first order slope of the decay of contact angle started to increase when the TiN ratio became more then 11%. This slope continued to increase gradually then stabilized when the TiN ratio was between 21% and 28%. The decrease in the value of contact angle, with time, is the result of two phenomena: first, the direct photocatalytic degradation of the oleic acid layer by the top thin layer of TiO_2 photocatalyst. Secondly, the photo induced hydrophilicity of the TiO_2. It is interesting to investigate the wettability and compare it with the results of the photocatalytic measurements, because the catalytic reaction could be drastically affected by the quality of the interface between the catalyst and the dye.

The study of the photocatalytic activity was realized by following the degradation of an aqueous solution of Rhodamine B dye (initial concentration of C^0=5 ppm), Fig. 9 shows the photocatalytic efficiency on the dye's degradation during irradiation time of 2 hours and 8 hours for white light and visible light, respectively. Without photocatalyst, the photo bleaching of Rhodamine B was less than 5% after 3 hours under white light irradiation.

Under visible light irradiation, all the bilayer samples showed higher photocatalytic activity as compared to pure TiO_2, the maximum photocatalytic efficiency was achieved with the samples prepared at TiN ratio between 21% and 28% in the case of 18 bilayers but also in the case of the 9 bilayers. This result is consistent with the observation of the photoelectrochemical measurements and the evolution of the hydrophillicity under photo irradiation.

Under white light, lower TiN ratio (TiN≤11%) gave less photocatalytic efficiency as compared to pure TiO_2, but when nominal ratio of TiN exceeded 16%, the UV light catalytic activity increased steadily for the 9 and 18 bilayers and presented a maximum catalytic efficiency for TiN ratio between 21% and 28%. This means that TiN layers impeded in TiO_2 can enhance the total photocatalytic activity as compared to pure TiO_2 when nominal TiN ratio is more than 16%, without reducing the UV photoactivity. This last result is interesting because, although, nitrogen doping is responsible for the enhancement of the visible light photocatalytic activity of N doped TiO_2, many authors reported a partial reduction in the UV photocatalytic activity when doping nitrogen in TiO_2 [45]. However, the bilayer strategy of TiN/TiO_2 has confirmed an enhancement of the visible light activity as compared to pure TiO_2 without any dramatic reduction of the UV photoactivity.

A representative curve of the decay rates for both 9 and 18 bilayers have been plotted in Fig.10 (more details and discussions are presented in the supplementary section). The overall trend declines exponentially with the time indicating a typical first order kinetics $C = C^0 e^{(-k.t)}$, where C^0, C and k are the initial concentration of the dye (5 ppm), the concentration at the instant t and the rate constant, respectively. The decay rate constant was calculated from the slope by plotting $\ln(C^0/C)$ *vs* time using an appropriate linear regression. Table 3 regroups the calculated rates for the different TiN loadings in the presence of the UV light k_{UV} and visible light alone k_{vis}. Most of the TiO_2/TiN bilayers showed improved degradation kinetic as compared to pure TiO_2, especially the bilayer coatings having higher TiN percentage. The decay rate is improved more than two times with the bilayers, having 21% and 28% nominal ratio of TiN, as compared to pure TiO_2. More interestingly, the half-life time of Rhodamine B was significantly reduced in the presence of the bilayer coatings as compared to pure TiO_2 (see the supplementary section). For instance, the half-life time was reduced from 142 min (for TiO_2) to 44 min, 51 min and 82 min for the 9 bilayers having TiN ratio of 28%, 21% and 16%, respectively. For the 18 bilayers, the half-life time was reduced to 51min, 67 min and 112 min, respectively, with the bilayers having TiN ratio of 28%, 21% and 16%.

Unlike the photo-electrochemical measurements, the photocatalytic activity seems to be less sensitive to the variation of thickness of the TiN layer for higher ratios of TiN (more than 21%). This difference in behavior of photo responses could be explained by the distinct mechanism of each activity. In fact, under sufficient bias, good photo-electrochemical activity

requires maximum charge density and minimum recombination in the bulk of the bilayer coating, this implies that all the photo generated electron-hole pairs (on the surface and in the bulk) should participate in generating the photocurrent. However, photocatalysis is a surface reaction that takes place under no external biasing. Thus, only the superficial photo generated electron-holes pairs are mainly responsible for the photocatalytic efficiency of the semiconductor.

4.7. Effect of the TiN layer on the charge lifetime

We can complete the model proposed in section 3 by investigating the charge generation within the bilayers as compared to pure TiO_2. The density of holes that are near the TiO_2/TiN interface should be different from that without the TiN layer. Also, the photo generation of carriers takes place in the volume of the photoactive material, but the photoreactions occur at the surface of the thin film, so we are more concerned with the total amount of charge that reaches to the surface of the semiconductor.

The above analytical section didn't reveal either N—Ti—O, Ti—N—O nor Ti—O—N bondings within TiO_2, for the studied bilayer coatings. Thus, we can assume that the generation of electron–hole pairs in pure TiO_2 thin films and bilayer films are the same, because the TiN layers are loaded on titania and there is no nitrogen doping within the TiO_2 layers at this low deposition pressure (see Fig.4 (c)). The enhanced visible light activity could be probably explained by the presence of some defects and/or energy levels in the band gap of TiO_2.

For a pure TiO_2, the effective hole density $\rho_{h.1}$ is given by, $\rho_{h.1} = G_h \times \tau_1$, where G_h is the generation rate of holes and τ_1 is the effective lifetime of the photogenerated holes in the pure TiO_2 thin film, which is determined by many different recombination processes. We can express the effective lifetime of the photo generated holes as, $\frac{1}{\tau_1} = \frac{1}{\tau_h} + \frac{1}{\tau_{t.1}} + \frac{1}{\tau_{CS.1}}$, where τ_h is the hole life time before direct band recombination, and $\tau_{t.1}$ is the time corresponding to the electron and hole trapping in the defect states and $\tau_{CS.1}$ is a time characteristic of the charge separation. With the presence of TiO_2/TiN interface, a space charge can be created in the TiO_2 layers (as discussed in section 3), this space charge corresponds to the region of the band bending and is characterized by $\tau_{CS.2}$ with $\tau_{CS.2} > \tau_{CS.1}$. Also, more electrons could be trapped by the TiN layer with a characteristic time of $\tau_{t.2} > \tau_{t.1}$, then the effective lifetime of

the photogenerated holes becomes $\frac{1}{\tau_2} = \frac{1}{\tau_h} + \frac{1}{\tau_{t.2}} + \frac{1}{\tau_{CS.2}}$ with $\tau_2 > \tau_1$, then the new effective hole density $\rho_{h.2}$ is given by, $\rho_{h.2} = G_h \times \tau_2$. This is directly correlated to the increases in the transient time constant τ as discussed in the previous section (Table 2). Here we assumed that G_h is the same in both cases as nitrogen is not doped in TiO_2.

5. Conclusions

Stacks composed of TiO_2/TiN bilayers were fabricated and characterized to determine their crystalline, compositional and photoactive properties. Deposition parameters have been chosen to produce stoichiometric 9 and 18 TiN/TiO_2 bilayers having different TiN/TiO_2 ratios, with well-defined Schottky barriers, however, the presence of the Ohmic contact cannot be excluded. These multistack films were compared with pure TiO_2 films with the same total thickness. The photo-electrochemical results showed that the thickness of the layers (TiN/TiO_2 ratio) plays an important role in the charge generation and charge separation properties within each film, as well as the visible light photo-activity, which is absent in undoped TiO_2 thin films. Interestingly, the optimal deposition conditions are estimated to reduce the recombination rate between the photo-induced electron-holes up to 10 times using this design, but the thickness of each TiN layer should not exceed a limiting value. This study has shown the ability to tailor nitrogen in TiO_2 films with controllable physicochemical properties and photoactive performance, the deposition parameters should be tuned depending on the type of application of the desired film.

Acknowledgements

The authors would like to thank the European project NATIOMEM and the French Ministry of Research and High Education for funding the mobility of the researchers

References

[1] A. Fujishima, X. Zhang, D.A. Tryk, *Surf. Sci. Rep.* **63** (2008) 515–582.

[2] W. Choi, A. Termin, M. Hoffman, *J. Phys. Chem.* **98** (1994) 13669–13679.

[3] T. Umebayashi, T. Yamaki, S. Yamamoto, Q. Miyashita, S. Tanaka, T. Sumita, K. Asai, *J. Appl. Phys.* **93** (2003) 5156–5160.

[4] H. Tong , S. Ouyang , Y. Bi, N. Umezawa , M. Oshikiri , J. Ye, *Adv. Mater.* **24** (2) (2012) 229–251.

[5] T. Umebayashi, T. Yamaki, H. Itoh, K. Asai, *Appl. Phys. Lett.* **81** (2002) 454–456.

[6] W. Ren, Z. Ai, F. Jia, L. Zhang, X. Fan, Z. Zou, *Appl. Catal., B* **69** (2007) 138–144.

[7] R. Apetrei, C. Catrinescu, D. Mardare, C. M. Teodorescu, D. Luca, *Thin Solid Films* **518** (2009) 1040–1043.

[8] R. Asahi, T. Morikawa, T. Ohwaki, K. Aoki, Y. Taga, *Science* **293** (2001) 269–271.

[9] S. Hamad, J.C. Gonza, A. Barranco, J.P. Espino, J. Cotrino, *J. Phys. Chem., C* **114** (2010) 22546–22557.

[10] C. Lee, L. Lin, K. Tsai, R. Vittal, K. Ho, *J. Power Sources* **196** (2011) 1632–1638.

[11] H. Fakhouri, J. Pulpytel, W. Smith, A. Zolfaghari, H.R. Mortaheb, F. Meshkini, R. Jafari, E. Sutter, F. Arefi-Khonsari, *Appl. Catal., B* **144** (2014)12–21.

[12] S. Higashimoto, N. Kitahata, K. Mori, M. Azuma, *Catal. Lett.* **101** (2004) 49–51.

[13] W. Smith, Y. Zhao, *J. Phys. Chem. C* **112** (2008) 19635–19641.

[14] Z. Wu, D. Lee, M. Rubner, R. Cohen, *Small* **3** (2007) 1445-1451.

[15] W. Smith, Y. Zhao, *Catal. Commun.* **10** (2009) 1117–1121.

[16] O. Carp, C.L. Huisman, A. Reller, *Prog. Solid State Chem.* **32** (2004) 33–177.

[17] W. Smith, H. Fakhouri, J. Pulpytel, F. Arefi-Khonsari, *J. Appl. Phys.* **111** (2012) 024301 1–10.

[18] Y. Jin, Y.G. Kim, J. H. Kim, D.K. Kim, *J. Korean Ceram. Soc.* **42** (7) (2005) 455–460.

[19] A. Didden, H. Battjes, R. Machunze, B. Dam, R. Krol, *J. Appl. Phys.* **110** (2011) 033717 1–7.

[20] N. Fuke, A. Fukui, A. Islam, R. Komiya, R. Yamanaka, H. Harima, L. Han, *Sol. Energ. Mat. Sol. Cells* **93** (2009) 720–724.

[21] D. Scanlon, C. Dunnill, J. Buckeridge, et al., *Nat. Mater.* **12** (2013) 798–801.

[22] A Subrahmanyam, K Biju, P Rajesh, K Jagadeesh Kumar, M Raveendra Kiran, *Sol. Energ. Mat. Sol. Cells* **101** (2012) 241–248.

[23] T. Cai, Y. Liao, Z. Peng, Y. Long, Z. Wei, Q. Deng, *J. Environ. Sci.* **21** (2009) 997–1004.

[24] H. Haick, Y. Paz, *J. Phys. Chem. B* **107** (2003) 2319–2326.

[25] N. Martin, R. Sanjinés, J. Takadoum, F. Lévy, Surf. Coat. Tech. 142 (2001) 615-620.

[26] A. Trenczek-Zajac, M. Radecka, K. Zakrzewska, A. Brudnik, E. Kusior, S. Bourgeois, M.C. Marco de Lucas, L. Imhoff, *J. Power Sources* **194** (2009) 93–103.

[27] D. Won, C. Wang, H. Jang, D. Choi, *Appl. Phys. A* **73** (2001) 595–600.

[28] M. Wong, H. Chou, T. Yang, *Thin Solid Films* **494** (2006) 244–249.

[29] J. Liao, H. Chen, C. Chang, S. Chiu, Z. Chen, *Thin Solid Films* **515** (2006) 176–185.

[30] Y. Li, M. Ma, X. Wang, Z. Li, *Surf. Coat. Tech.* **204** (2010) 1353–1358.

[31] G. He, L. Zhang, G. Li, M. Liu, X. Wang, *J. Phys. D: Appl. Phys.* **41** (2008) 045304 1–9.

[32] H. Matsui, H. Tabata, *J. Appl. Phys.* **97** (2005) 123511 1–8.

[33] B. Avasarala, P. Haldar, *Electrochim. Acta* **55** (2010) 9024–9034.

[34] S. Lee, I. Cho, D.K. Lee, D.W. Kim, T.H. Noh, C.H. Kwak, S. Park, K.S. Honga, J.K. Lee, H.S. Jung , *J. Photochem. Photobiol., A* **213** (2010) 129–135.

[35] A.V. Emeline, V.N. Kuznetsov, V.K. Rybchuk, N. Serpone, Review, *Int. J. Photoenerg.* (2008) 258394 1–19.

[36] H.M. Yates, M.G. Nolan, D.W. Sheel, M.E. Pemble, *J. Photochem. Photobiol., A* **179** (2006) 213–223.

[37] C. Di Valentin, E. Finazzi, G. Pacchioni, A. Selloni, S. Livraghi, M.C. Paganini, E. Giamello, *Chem. Phys.* **339** (2007) 44–56.

[38] H. Kawasaki, T. Ohshima, Y. Yagyu, Y. Suda, SI. Khartsev, AM. Grishin, *J. Phys.: Conf.* Ser. **100** (2008) 012038 1–4.

[39] R. Parra, A. Arango, J. Palacio, *Dyna* **77** (163) (2010) 64–74.

[40] M.A. Baker, H. Fakhouri, R. Grilli, J. Pulpytel, W. Smith, F. Arefi-Khonsari, *Thin Solid Films* **552** (2014) 10–17.

[41] N. Laidani, P. Cheyssac, J. Perrière, R. Bartali, G. Gottardi, I. Luciu, V Micheli, *J. Phys. D: Appl. Phys.* **43** (2010) 485402 1-11.

[42] H Fakhouri, D Ben Salem, O Carton, J Pulpytel, F Arefi-Khonsari, *J. Phys. D: Appl. Phys.* **46** (26) (2014) 265301 1–11.

[43] Z. Zhang, J. Goodall, D. Morgan, S. Brown, R. Clark, J. Knowles, N. Mordan, J. Evans, A. Carley, M. Bowker, J. Darr, *J. Eur. Ceram. Soc.* **29** (2009) 2343–2353.

[44] A. Fujishima, K. Honda, *Nature* **238** (1972) 37–38.

[45] J. Wang, D.N. Tafen, JP. Lewis, Z. Hong, A. Manivannan, M. Zhi, M. Li, N. Wu, *J. Am. Chem. Soc.* **131** (34) (2009) 12290–12297.

Table 1. Estimated thickness of each TiO_2 and TiN layer in the 9 and 18 bilayer deposited at different TiN/TiO_2 thickness ratio.

Table 2. Calculated values of the time constant τ (sec) for different ratios of TiN in the 9 and 18 bilayers.

Table 3. Calculated values of the decay rate (min^{-1}) of Rhodamine B, for different ratios of TiN in the 9 and 18 bilayers, under visible light alone (k_{vis}) and in presence of the UV irradiations (k_{UV}).

Fig. 1. Electronic band structure of (a) two individual layers of TiN and TiO_2 and (b) one bilayer of TiO_2/TiN showing the formation of a Schottky barrier. VB, CB, E_{f_1}, E_{f_2} and E_f correspond to the valence band, the conductive band, Fermi level of TiO_2, Fermi level of TiN and Fermi level of the bilayer, respectively.

Fig. 2. XRD patterns of (a) the 9 bilayer film and (b) the 18 bilayer thin films deposited on silicon. The patterns were taken after annealing for 2 hours at $T_A = 450^oC$. The pattern of pure TiO_2 coating is presented as a reference.

Fig. 3. Variation of the crystal size of the anatase phase as calculated from Scherer formula for the 9 and 18 bilayers coatings vs the ratio of TiN.

Fig. 4. XPS spectra of (a) Ti 2p including 1/2 and 3/2 spins, (b) O1s core level spectra and (c) N 1s core level spectra, for the 9 and the 18 bilayers having fixed TiN ratio (21%) as compared to the pure TiO_2 thin coating.

Fig. 5. An example of fitted O 1s spectra for the 18 bilayer, TiN ratio was 21% as compared to TiO_2 thickness.

Fig. 6. Photocurrent generated at 0.5V/(AgCl/Ag) for (a) the 18 bilayers (zoomed on the visible light range in (b,))and (c) the 9 bilayers (zoomed on the visible light range in (d)), with different TiN ratios of loaded layer within the photoactive film. (τ is a transient time constant).

Fig. 7. Photocurrent generated at 0.5V/(AgCl/Ag) for (a) the 9 bilayers and (b) the 18 bilayers, vs TiN loaded layer ratio as compared to pure TiO_2, under white (black) and visible (red) irradiations.

Fig. 8. Variation of the contact angle of water droplet on the surface of contaminated TiO_2/TiN bilayers as a function of TiN ratio and the irradiation time under white light (UV+visible). The surface of the coatings was initially contaminated with oleic acid at room temperature.

Fig.9. Evaluation of the photocatalytic efficiency, under white light (UV+visible) and visible light alone at room temperature, on the degradation of Rhodamine B (initial concentration 5 ppm, 5 ml), using the different samples of TiO_2/TiN bilayers (surface 0.9x2.5 Cm^2) as a function of TiN ratio. Total irradiation time was 2 h for white light and 8 h for visible light. For comparison, the photocatalytic efficiency of pure TiO_2 is presented as well: in grey (UV+visible light) and orange (visible light).

Fig. 10. Example of the time profile describing the degradation kinetic of Rhodamine B (initial concentration 5 ppm, 5 ml) in the presence of the 9 and 18 bilayers (surface 0.9x2.5 Cm^2) having different TiN/TiO_2 ratio, under UV+visible light and at room temperature. More details can be seen in the supplementary section.

TiN/TiO_2 nominal ratio →		*5 %*	*11 %*	*16 %*	*21 %*	*28 %*
9 bilayers	TiO_2 (nm)	50	47	45	42	38
	TiN (nm)	3	6	8	11	15
18 bilayers	TiO_2 (nm)	26	24	23	21	20
	TiN (nm)	2	3	4	6	8

Table 1

	5%	11%	16%	21%	28%
9 bilayer	2.1	2.0	9.9	14.2	11.0
18 bilayer	1.6	2.5	8.7	14.7	15.9

Table 2

	9 Bilayers		18 Bilayers	
	$k_{UV} \times 10^3$	$k_{vis} \times 10^3$	$k_{UV} \times 10^3$	$k_{vis} \times 10^3$
TiO_2	5.02	0.08		
5%	4.79	0.116	2.69	0.11
11%	5.47	0.273	3.94	0.15
16%	8.02	0.46	6.11	0.35
21%	13.37	0.491	10.26	0.63
28%	13.57	0.388	12.63	0.61

Table 3

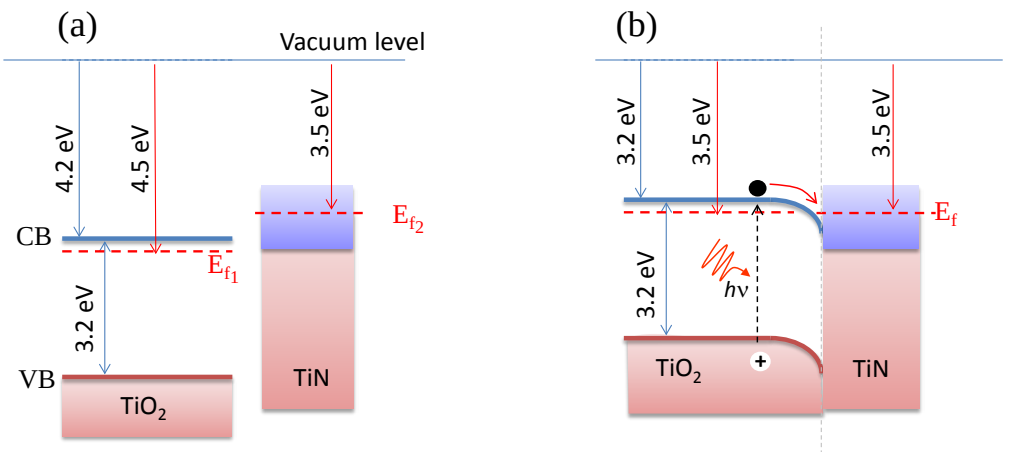
(a)
Vacuum level
4.2 eV
4.5 eV
3.5 eV
CB
E_{f_2}
E_{f_1}
3.2 eV
VB
TiO_2
TiN
(b)
3.2 eV
3.5 eV
3.5 eV
E_f
3.2 eV
hv
TiO_2
+
TiN

Figure 1

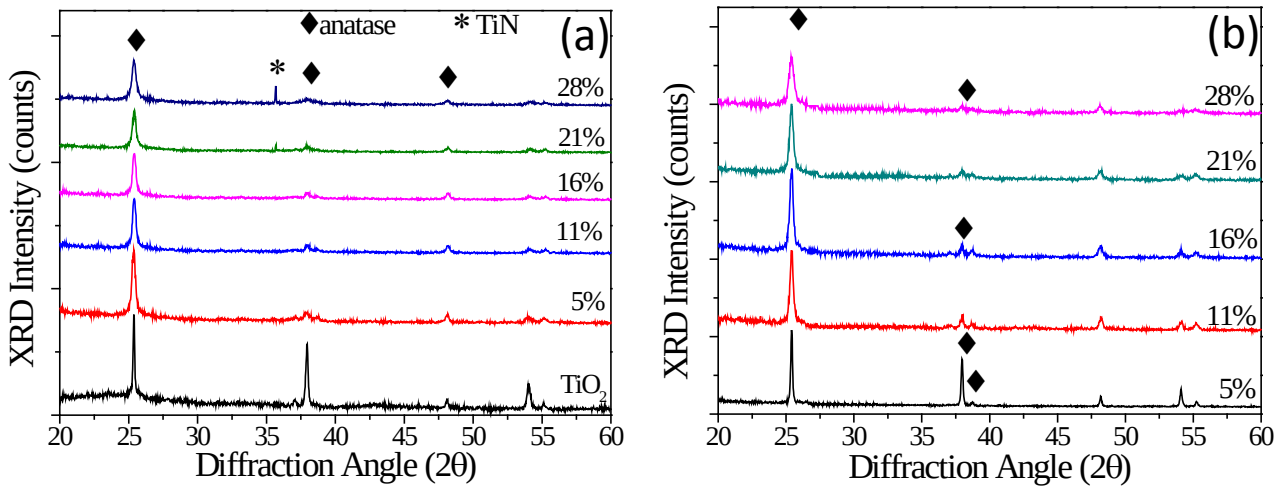
(a)
anatase
TiN
28%
21%
16%
11%
5%
TiO2
XRD Intensity (counts)
Diffraction Angle (2θ)
20
25
30
35
40
45
50
55
60
(b)
28%
21%
16%
11%
5%
XRD Intensity (counts)
Diffraction Angle (2θ)

Figure 2

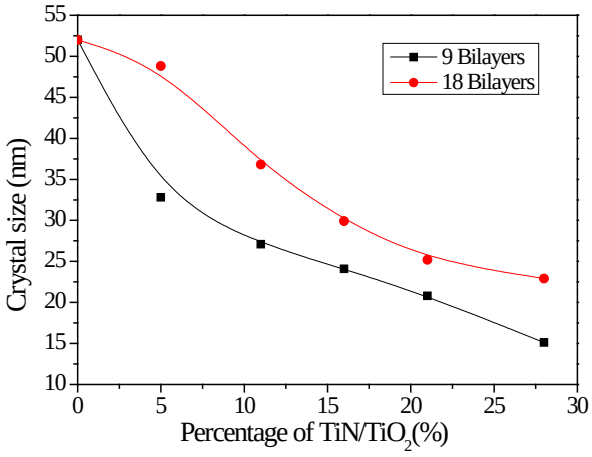
9 Bilayers
18 Bilayers
Crystal size (nm)
Percentage of TiN/TiO2(%)
55
50
45
40
35
30
25
20
15
10
0
5
10
15
20
25
30

Figure 3

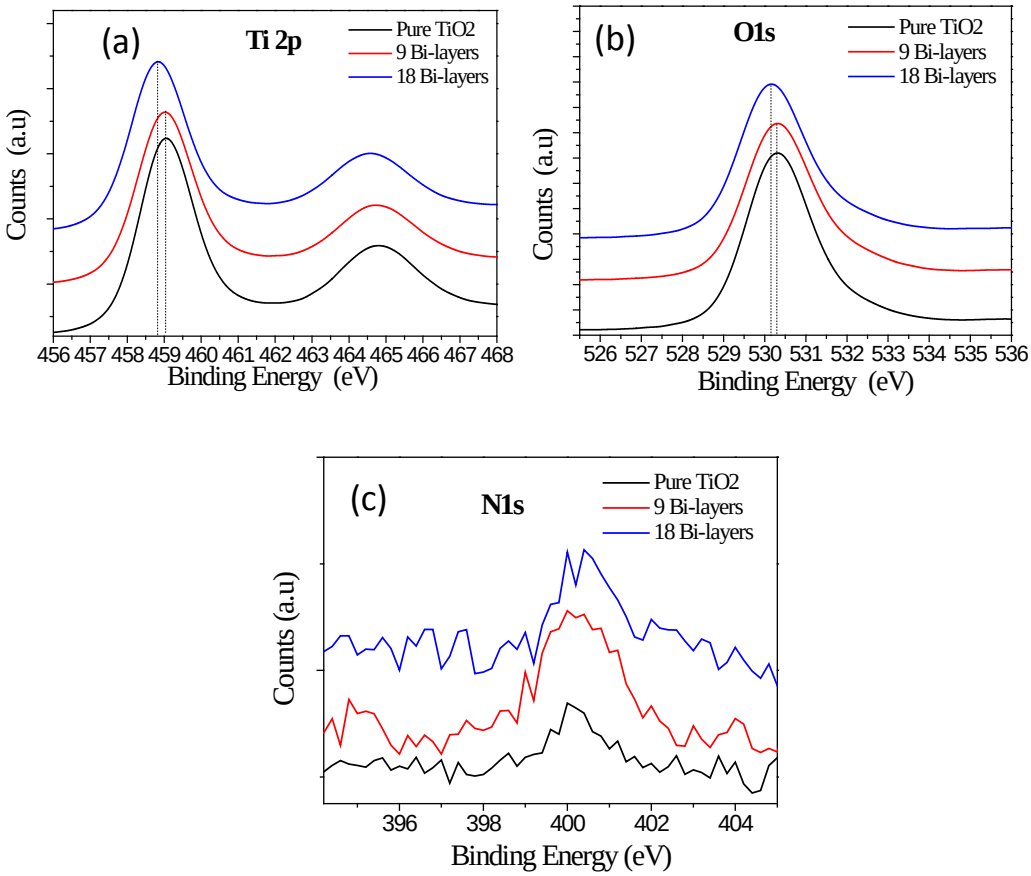
(a)
Ti 2p
Pure TiO2
9 Bi-layers
18 Bi-layers
Counts (a.u)
456 457 458 459 460 461 462 463 464 465 466 467 468
Binding Energy (eV)
(b)
O1s
Pure TiO2
9 Bi-layers
18 Bi-layers
Counts (a.u)
526 527 528 529 530 531 532 533 534 535 536
Binding Energy (eV)
(c)
N1s
Pure TiO2
9 Bi-layers
18 Bi-layers
Counts (a.u)
396 398 400 402 404
Binding Energy (eV)

Figure 4

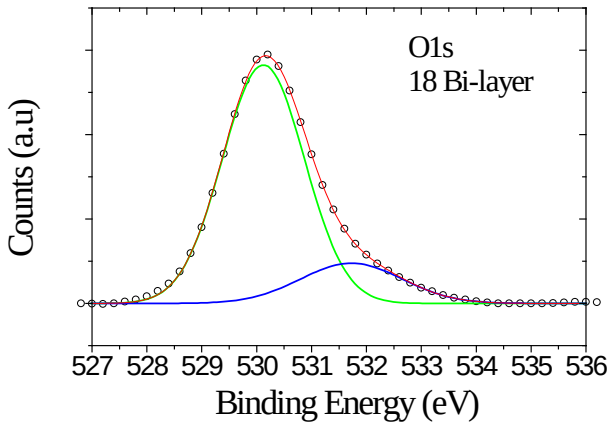
O1s
18 Bi-layer
Counts (a.u)
527 528 529 530 531 532 533 534 535 536
Binding Energy (eV)

Figure 5

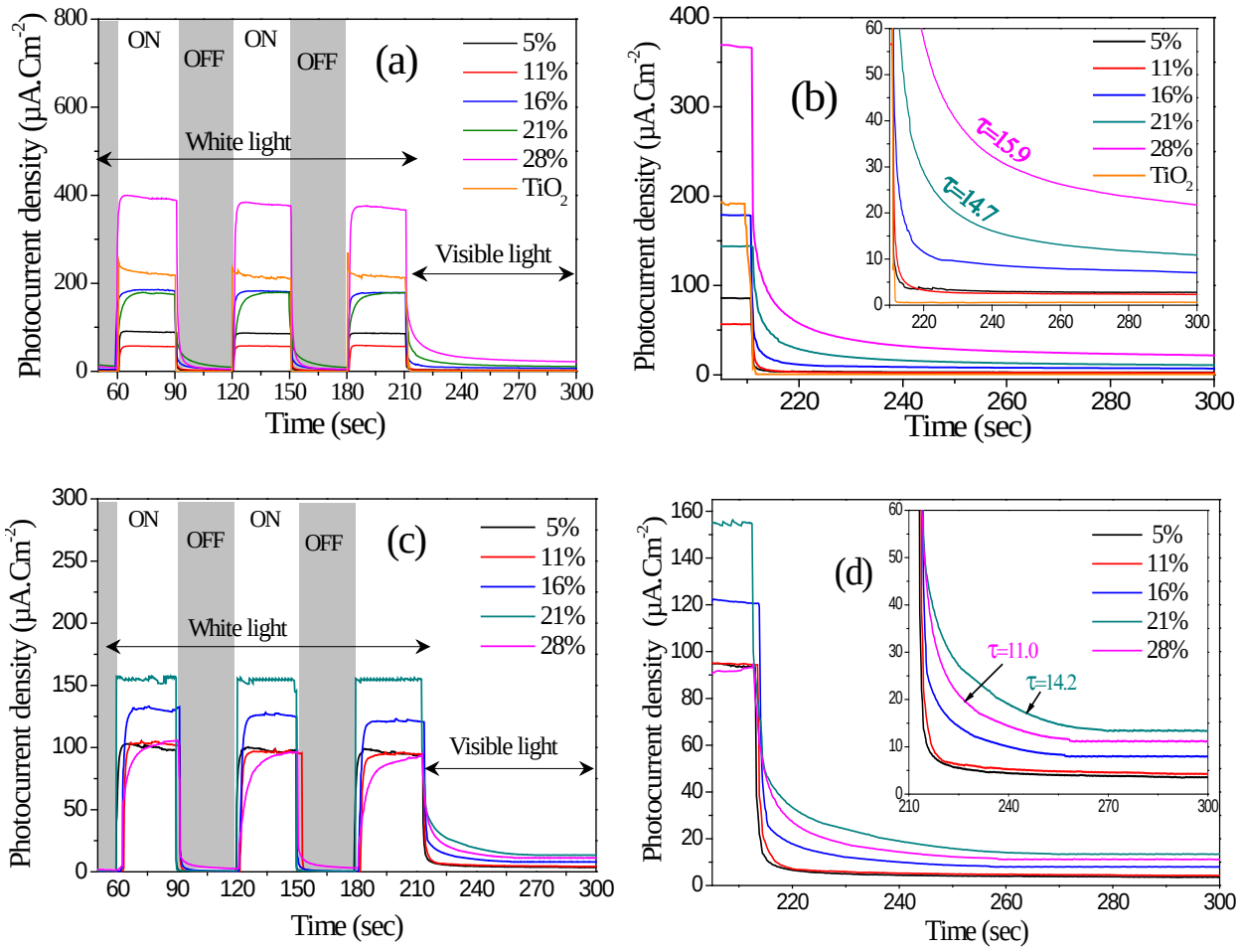
(a)
ON
OFF
ON
OFF
White light
Visible light
5%
11%
16%
21%
28%
TiO2
Photocurrent density (μA.Cm-2)
Time (sec)
(b)
τ=15.9
τ=14.7
(c)
(d)
τ=11.0
τ=14.2

Figure 6

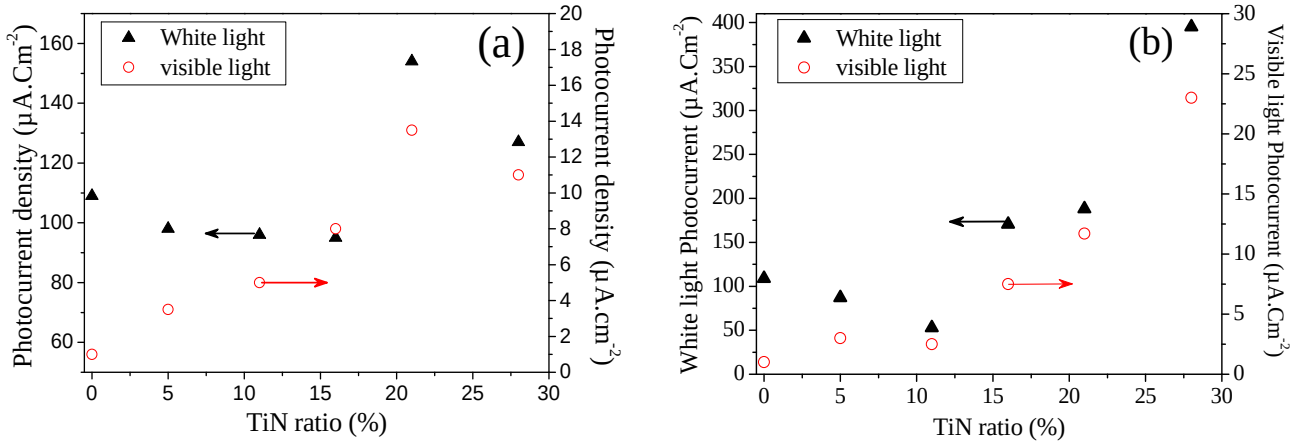
White light
visible light
(a)
Photocurrent density (µA.Cm-2)
Photocurrent density (µA.cm-2)
TiN ratio (%)
White light
visible light
(b)
White light Photocurrent (µA.Cm-2)
Visible light Photocurrent (µA.Cm-2)
TiN ratio (%)

Figure 7

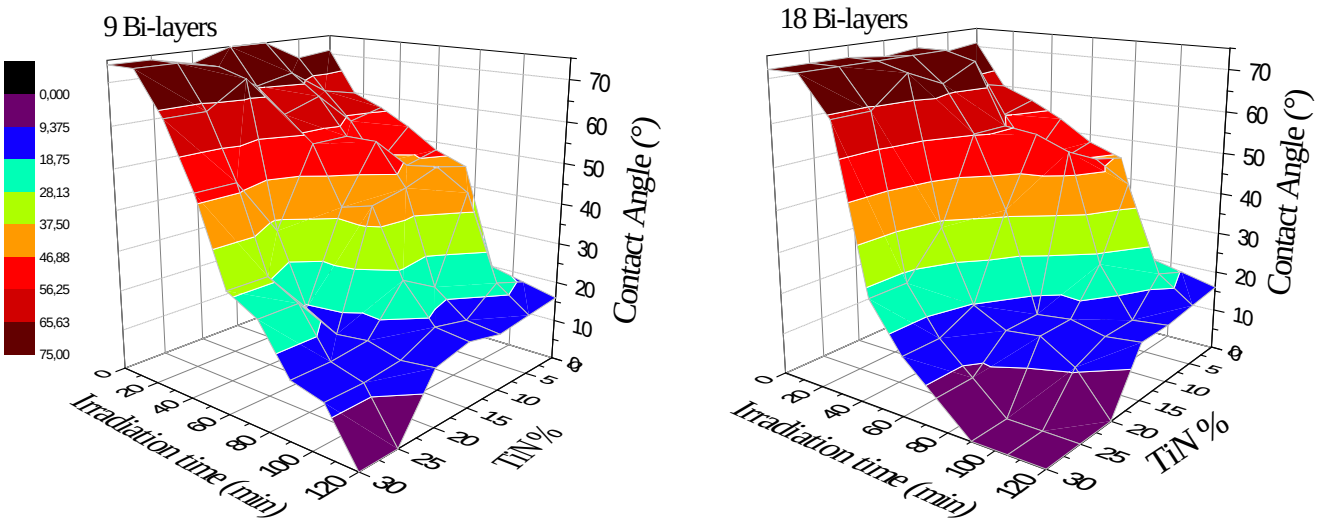
9 Bi-layers
0,000
9,375
18,75
28,13
37,50
46,88
56,25
65,63
75,00
Contact Angle (°)
Irradiation time (min)
TiN%
18 Bi-layers
Contact Angle (°)
Irradiation time (min)
TiN%

Figure 8

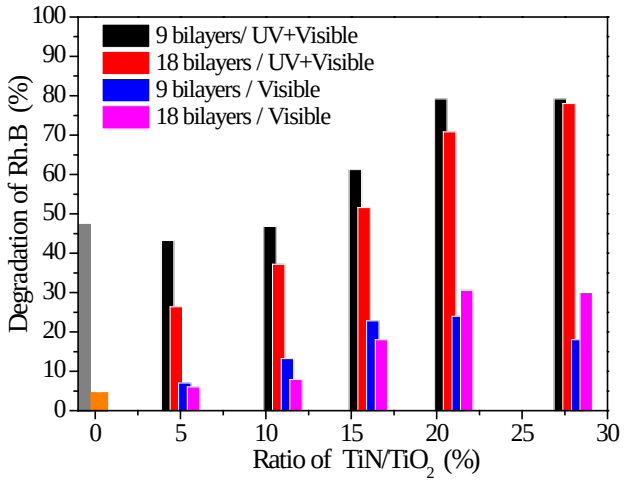
9 bilayers/ UV+Visible
18 bilayers / UV+Visible
9 bilayers / Visible
18 bilayers / Visible
Degradation of Rh.B (%)
Ratio of TiN/TiO2 (%)
0
10
20
30
40
50
60
70
80
90
100
0
5
10
15
20
25
30

Figure 9

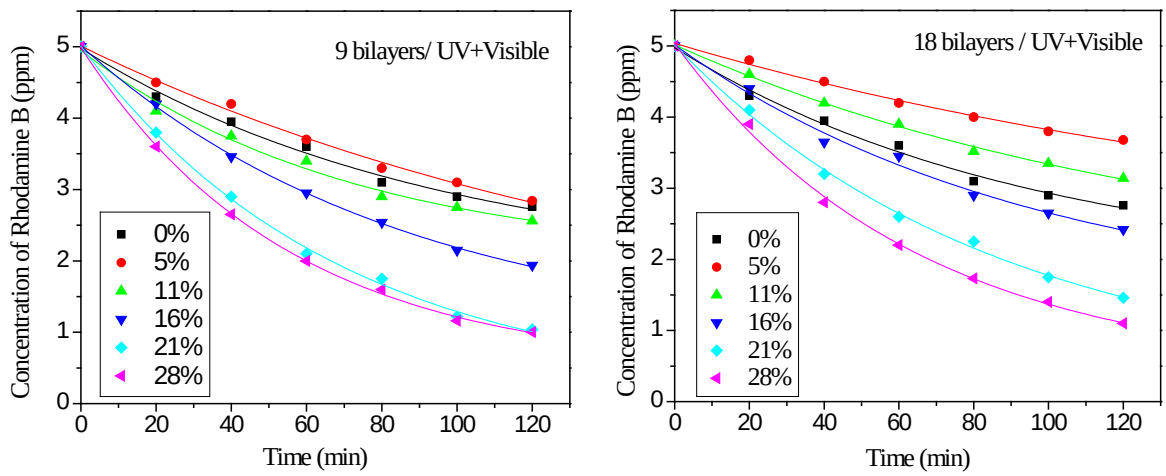
9 bilayers/ UV+Visible
18 bilayers / UV+Visible
Concentration of Rhodamine B (ppm)
Time (min)
0%
5%
11%
16%
21%
28%
0
1
2
3
4
5
0
20
40
60
80
100
120

Figure 10